ACS OMEGA

http://pubs.acs.org/journal/acsodf

Article

Embedded Direct Ink Writing 3D Printing of UV Curable Resin/Sepiolite Composites with Nano Orientation

Hoon Kim, Jaehwan Kim, Kwang-Hyun Ryu, Jiho Lee, Hyun-Joong Kim,* Jinho Hyun, and Jaseung Koo

Cite This: *ACS Omega* 2023, 8, 23554−23565

Read Online

ACCESS | Metrics & More | Article Recommendations | Supporting Information

ABSTRACT: Among the various 3D printing methods, direct ink writing (DIW) through extrusion directly affects the microstructure and properties of materials. However, use of nanoparticles at high concentrations is restricted due to difficulties in sufficient dispersion and the deteriorated physical properties of nanocomposites. Thus, although there are many studies on filler alignment with high-viscosity materials with a weight fraction higher than 20 wt %, not much research has been done with low-viscosity nanocomposites with less than 5 phr. Interestingly, the alignment of anisotropic particles improves the physical properties of the nanocomposite at a low concentration of nanoparticles with DIW. The rheological behavior of ink is affected by the alignment of anisotropic sepiolite (SEP) at a low concentration using the embedded 3D printing method, and silicone oil complexed with fumed silica is used as a printing matrix. A significant increase in mechanical properties is expected compared to conventional digital light processing. We clarify the synergistic effect of the SEP alignment in a photocurable nanocomposite material through physical property investigations.

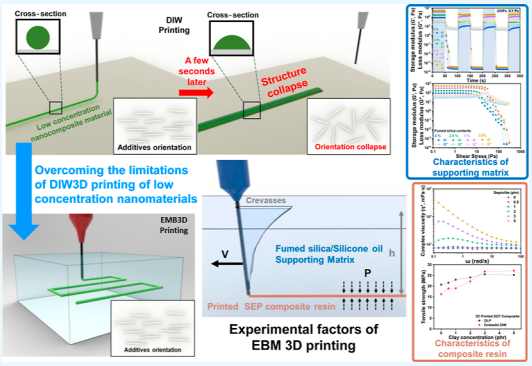

1. INTRODUCTION

Additive manufacturing, which enables the design and direct printing of three-dimensional (3D) objects, has revolutionized the possibilities for research into the industry and advanced materials.[1,2] 3D printing of polymers has been largely categorized into two: extrusion molding by applying heat to a polymer and photo-curing with a resin having photolabile groups. However, new reaction-based technologies, such as e-beam, have been developed, which allow extrusion-based polymer 3D printing without heat supply and are in situ cured. In addition, they have the potential to acquire functionality by applying various kinds of nanomaterials, which can be broadly applied in industrial engineering.[3−17]

Among nanomaterials having excellent physical properties, a nanoclay is especially suitable for industrial applications due to its affordable price.[18] Sepiolite (SEP), a hydrated magnesium silicate with the half-unit-cell formula of $Mg_8Si_{12}O_{30}(OH)_4 \cdot 12H_2O$, is one of the most widely used nanoclays as a reinforcing filler. A single SEP fiber has dimensions of 0.2−4 μm in length, 10−30 nm in width, and 5−10 nm in thickness.[19,20] It has a needle-like or fiber-like morphology, comprising several blocks and tunnels oriented parallel to the fiber direction.

Direct ink writing (DIW) is an extrusion-based 3D printing technology that enables the programmable assembly of 3D architectures. Unlike conventional lithography such as laser-based polymerization or epitaxial assembly technology, it has been applied to a wide range of materials in inorganic and organic chemistry.[21−31] Despite the easy extrusion of ink materials, it is difficult to develop a viscoelastic ink that maintains its shape after its extrusion.[32] In normal conditions, high concentrations of nanomaterials in ink are critical to achieve a self-supporting structure after printing through the needle. The higher the concentration of nanomaterials, the better the resolution of printing can be achieved.[33−37] In particular, DIW of cellulose nanocrystal-incorporated inks has been actively investigated because cellulose nanocrystals, an anisotropic building block, can be a filler of nanocomposites with shear-induced alignment during the extrusion process through the nozzle in DIW.[38,39] The nanocomposite requires an optimal concentration of nanofillers to obtain sufficient viscoelastic properties in the DIW process as well as the improvement of the mechanical properties of the 3D products because the high concentration of nanofillers frequently deteriorates the physical properties of the composites by the slippage or inhomogeneity.[3,9,17,20,40,41]

It is critical to maximize the mechanical strength of nanocomposites by reinforcing them at low concentrations. DIW enables the improvement of the mechanical properties by aligning the nanofillers during the printing, but it is necessary

Received: February 21, 2023
Accepted: May 25, 2023
Published: June 20, 2023

Table 1. Formulation of the Acrylate/Clay Nanocomposite

composition[a]							
UV Resin[b]	PI(819)[c]	sample	printing method	sepiolite[c]	sample	printing method	sepiolite[c]
100	1	DLP Sep-0	DLP	0	EMB Sep-0	Embedded DIW	0
		DLP Sep-0.5		0.5	EMB Sep-0.5		0.5
		DLP Sep-1		1	EMB Sep-1		1
		DLP Sep-2		2	EMB Sep-2		2
		DLP Sep-3		3	EMB Sep-3		3
		DLP Sep-5		5	EMB Sep-5		5

[a]Total weight of the resin mixture was 225 g. [b]All the monomers were based on the weight percent. [c]Weight percent of the photoinitiator and clay was based on total monomer weight.

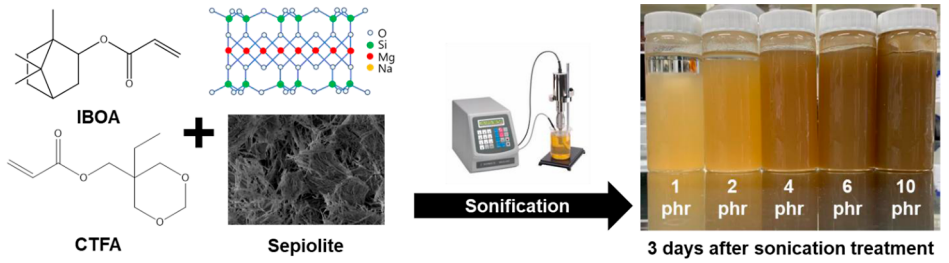

Figure 1. Photograph after the SEP was dispersed for 1 min with a sonicator tip at a power of 750 W in CTFA and IBOA monomers and then left for 3 days.

to use a low concentration of nanofillers. However, the low concentration of nanofillers in ink cannot produce the free-standing features due to insufficient viscoelastic characteristics. In recent years, a method has emerged to overcome the limitations of the DIW printing method by embedding the liquid features in a soft supporting matrix along a predefined omnidirectional printing path.[42,43] However, embedding 3D (EMB3D) printing requires complex consideration of the rheological properties and chemical interactions between the printing material and the supporting matrix.[44−47] For this reason, various trials and studies have been conducted in electronics and biotechnology to verify the feasibility of EMB3D printing.[46,48,49]

In this paper, we successfully printed a photocurable nanocomposite resin in which the nanoscale anisotropic SEP was applied at a low concentration using the EMB3D printing method. Silicone oil complexed with fumed silica was used as a printing matrix. The printed composite material significantly increased mechanical properties due to the dramatic increase in physical properties caused by the alignment of SEP nanocomposites during the passage through the printing nozzle. In order to clarify the reason for the synergistic effect with EMB3D printing, the physical properties of SEP nanocomposites printed in the silicon-fumed silica matrix were investigated by rheometry, mechanical analysis, dynamic mechanical analysis (DMA), transmission electron microscopy (TEM), scanning electron microscopy (SEM), and synchrotron ultra-small-angle X-ray scattering (U-SAXS). Besides, we specify the silica concentration of the matrix suitable for EMB3D printing, confirm the behavior and orientation of the SEP composite resin during the printing process, and establish the condition for exhibiting the directionality and synergistic effects of the nanocomposites.

2. MATERIALS AND METHODS

2.1. Materials. Diacrylate oligomer resins having acrylic groups at both ends (GR30860 and GR3060) were supplied by Graphy Inc. (Korea). Cyclic trimethylolpropane formal acrylate (CTFA) was supplied by Miwon Specialty Chemical Co., Ltd. (Korea). The monofunctional acrylated monomer of isobornyl acrylate (IBOA) was purchased from Evonik Industries AG (Germany). Bis(2,6-dichlorobenzoyl)-(4-propylphenyl)phosphine oxide (Irgacure 819) was obtained from BASF (Germany). SEP ($Mg_2H_2Si_3O_9{\cdot}xH_2O$) having a diameter of 10−30 nm and a length of 1−2 μm was purchased from Sigma-Aldrich (USA). Fumed silica was purchased from Sigma-Aldrich (USA) and silicone oil (KF-54) was purchased from Shin-Etsu (Japan).

2.2. Preparation of the Supporting Matrix. The supporting matrix for EMB3D printing was prepared by dispersing fumed silica in silicone oil. The fumed silica concentration of the silicone oil/fumed silica suspension was 1.5, 2.0, 2.5, 3.0, and 3.5%, and the total mass of the suspension was 40 g. Dispersion of fumed silica in silicone oil was performed by sonication for 180 s at an amplitude of 70% using a sonicator (VCS-130, Sonics & Materials Inc., USA) with a power of 130 W and a frequency of 20 kHz. The prepared silicone oil/fumed silica suspension was poured into a polystyrene Petri dish.

2.3. Preparation of Photocurable Resin and SEP Composite Resin. The photocurable resin and the photocurable SEP nanocomposite material used in this experiment were prepared in the ratio shown in Table 1. However, the oligomer resins (GR30860 and GR3060) were heated in an oven at 60 °C for 12 h to ensure fluidity and then blended. 50 g of CTFA and 50 g of IBOA were mixed, and SEP was added to the mixture under stirring (Table 1). The mixture was then sonicated for 1 min at 750 W. Finally, 1 phr of the photoinitiator was added to the mixture solution and degassed using a paste mixer. A photoinitiator is added after the sonification process such that no polymerization of monomers occurs during pre-treatment. In order to ensure that no polymerization occurs during pre-treatment, a pre-test was conducted, and the results showed no change in viscosity

https://doi.org/10.1021/acsomega.3c01165
ACS Omega 2023, 8, 23554−23565

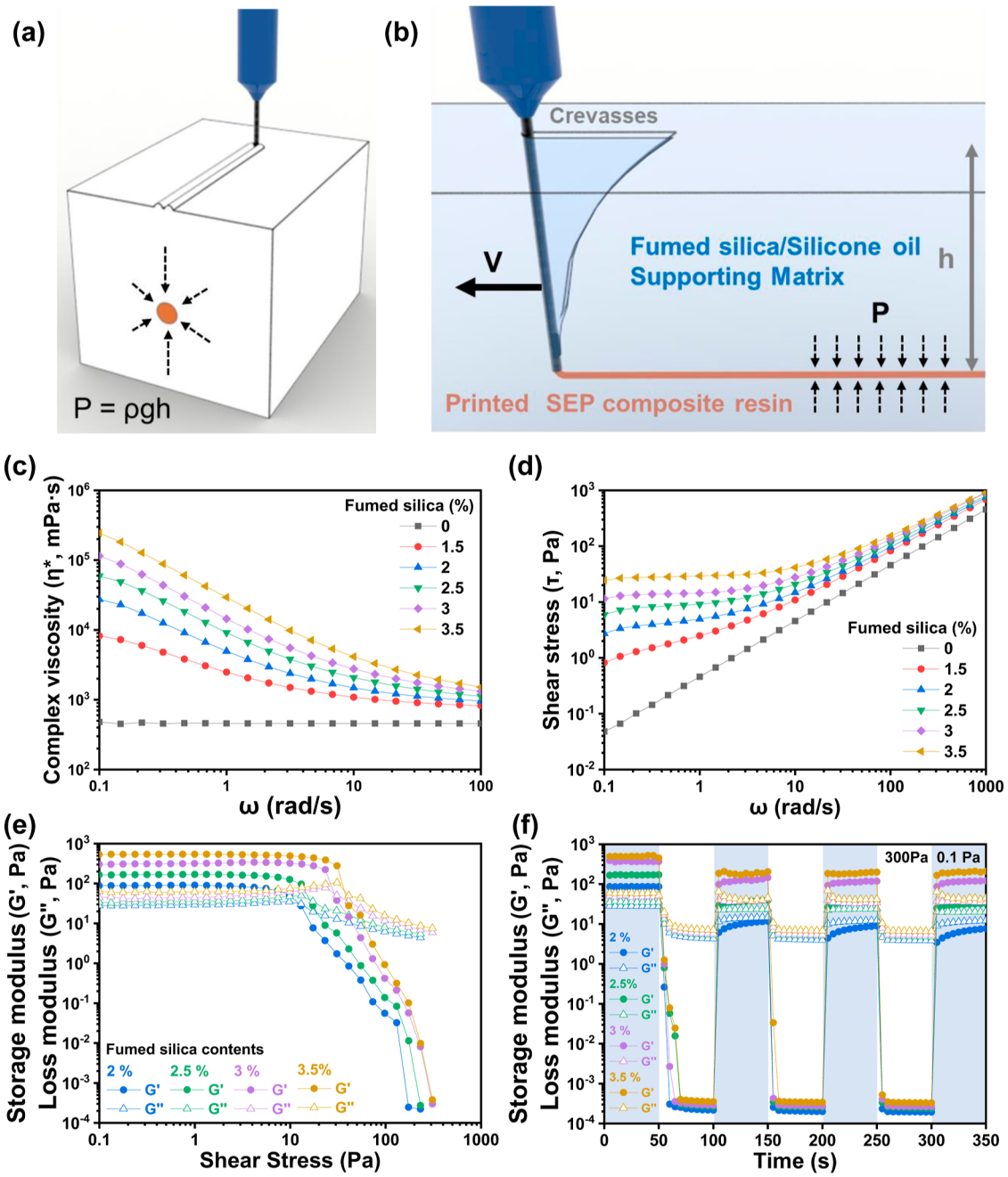

Figure 2. Schematic illustration of the crevasses formation condition according to the matrix yield stress. (a) Shape changes of printed ink cross-section due to the relationship between the CNF matrix yield stress and the hydrostatic pressure. (b) Hydrostatic pressure at the position where the nozzle passes through the CNF matrix. Rheological characterization of a silicone oil/fumed silica slurry supporter. (c) Viscosity of the supporter at different contents of fumed silica as a function of the angular velocity. (d) Shear stress of the supporter at different contents of fumed silica as a function of the angular velocity. (e) Storage and loss moduli of the supporter at different contents of fumed silica in stress sweeps. (f) Cyclic stress time sweep for 2, 2.5, 3, and 3.5 wt % supporting fumed silica/silicone oil gel. For cyclic stress, the shaded regions were at a low stress of 0.1 Pa and the unshaded regions were at a high stress of 200 Pa.

and FTIR results of the monomer before and after sonification. As shown in Figure 1, the mixture solution showed a very stable dispersion state even after 3 days of storage.

2.4. Preparation of Specimens. A DLP-type 3D printer (G PRINTER, Gooo3D, Korea) was used to prepare the specimen for tensile strength and DMA of composite resin materials. Tensile strength specimens were printed according to ASTM D638-5 (Standard Test Method for testing tensile strength for plastics and resin materials), and DMA samples were prepared in the size of 12.5 × 3 × 60 mm and printed with a 405 nm UV LED light source.

The SEP composite ink was printed in a supporting matrix using a custom-built DIW-3D printer. The 3D nozzle pathway was designed using the commercially available Rhinoceros software (Rhinoceros 5.0, Robert McNeel & Associates, Seattle, WA, USA). The designed 3D nozzle pathway models were translated into G-code instructions for deposition using slicing software (Cura, Ultimaker, Geldermalsen, The Netherlands). The SEP ink in a 5 mL syringe was printed in a

https://doi.org/10.1021/acsomega.3c01165
ACS Omega 2023, 8, 23554−23565

supporting matrix. The needle was inserted into the bottom center of the supporting matrix in the Petri dish, and the G-code was sent to the printer using the host software. The ink was extruded through a syringe needle with an inner diameter of 250 μm. The applied pressure was 45 psi and the printing speed was 10 mm/s.

The output was exposed to UV at 2 mW/cm^2 to stabilize the dimension. The post-curing of the printed features was performed by irradiating UV light for 5 min at 120,000 mJ/cm^2 using CureM U102H (Graphy Inc., Korea).

2.5. Characterizations. The rheological properties of fumed silica/silicone oil surrey were measured by a rheometer (MCR 302, Anton Paar Ltd., Austria). The diameter of the disposable parallel plate was 50 mm, the experimental temperature was 25 °C, the plate gap was set at 100 μm, the shear force for the step was 300 and 0.1 Pa, and the testing time was 50 s for each step (total 350 s). The diameter of the disposable parallel plate was 25 mm, the experimental temperature was 25 °C, the plate gap was set at 100 μm, and the angular velocity was 0.1−100 rad/s. To measure the photo-rheological properties of resin and the photocurable SEP resin composite, the shear rate was 0.01% and the radian was 10 rad/s. A UV LED with a wavelength of 365 nm was used, and the intensity was 15 mW/cm^2. Oscillation was carried out for 30 s, and then the material was UV irradiated for 300 s. The degree of shrinkage of the material was measured at a shear force of 0.1 N.

The tensile strength of the composite samples was measured using a UTM (AllroundLine Z010, Zwick, Germany) to confirm the changes in material properties and 3D printing effects with increasing SEP content and differences by a printing method. A crosshead speed of 5 mm/min was used during the measurements, and the mechanical properties were analyzed at room temperature (RT, ∼20 °C). Seven specimens of each composition were measured to calculate the margin of error.

In order to define the degree of orientation of SEP in the EMB3D-printed SEP nanocomposites from a morphological perspective, composite specimens were observed using TEM (JEM-2100F, JEOL Co., Japan). The TEM samples were prepared by slicing using Spurr resin.[50] In order to obtain TEM samples, the 3D-printed composite samples were impregnated with Spurr resin,[50] held for 24 h in vacuum conditions (−0.95 bar), and cured in an oven at 70 °C for 24 h. The cured sample was sliced using an ultramicrotome (EM UC7, Leica, Germany). The sample was loaded on a copper grid, and a carbon coating was applied for 30 s.

In order to confirm the effect of SEP inclusion on the fracture behavior of the polymer composite, the post-tensile-testing fracture surface of the EMB3D-printed samples was observed with field-emission SEM (FE-SEM, SUPRA 55VP, Carl Zeiss, Germany) at an acceleration voltage of 10 kV. Before the FE-SEM measurement, each sample was pre-coated with platinum (99.99% purity) by ion sputtering to eliminate electron charging.

DMA (Q800, TA Instrument, USA) was performed between −30 and 120 °C with a frequency of 1 Hz and a strain rate of 0.1% using the three-point bending method.

3. RESULTS AND DISCUSSION

3.1. Rheological Properties of the Matrix. In contrast to DIW, EMB3D printing uses a supporting matrix to stably print a material of low viscosity in the matrix, which maintains its shape after printing. Figure 2a,b explains the importance of the rheological properties of the matrix in EMB3D printing. Immediately after the nozzle passes, crevasses formed in the process of the printing collapse at the hydrostatic pressure (ρgh, where ρ is the density, g is the gravity, and h is the depth) from the bottom. If the yield stress of the matrix is too high, the matrix does not recover quickly, and the ink fills the crevasse changing the shape of the design. The rheological characteristics of matrices were investigated with the fumed silica/silicone oil slurry by varying the concentration to determine the suitable concentration of fumed silica for printing.

As the angular velocity increased, the fumed silica-added matrix showed shear-thinning behavior. Figure 2c,d shows that the shear-thinning behavior of the matrix becomes more obvious as the concentration of fumed silica increases. The compatibility between fumed silica and silicone oil is excellent, and nano-sized fumed silica has a high specific surface area, so only 0.5 wt % of the silicone oil showing Newtonian fluid changes rapidly into shear-thinning behavior. As the interaction between fumed silica particles and silicone oil and the distance between fumed silica particles decrease, higher yield stress occurs and the viscosity increases. This behavior resulted from the response of the matrix to the deformation that occurs in the process of printing as the nozzle passes through it. Therefore, it is important to find the appropriate yield characteristics. Yield stress corresponds to shear stress when the angular velocity is zero. Figure 3 also shows shear-thinning behavior and shows a stable response from 1 to 10 Hz. Therefore, it is evidence that it is reasonable to experiment under the condition of 1Hz.

It is important to understand the yield stress characteristics of the fumed silica/silicone oil matrix because the elastic modulus changes dramatically as the shear stress applied to the matrix increases. Oscillatory shear rheometry tests were performed at a frequency of 1 Hz to confirm the yield stress of the fumed silica/silicone oil matrix. Figure 2e shows the changes in the elastic and viscous moduli of the fumed silica/silicone oil matrix according to the change in the fumed silica content. As the fumed silica content increased, the elastic modulus and the range of solid-dominated shear stress increased. The yield stress is determined by the change in the storage modulus and the loss modulus and is confirmed by the shear stress value at the time when the storage modulus decreases.[43,47] As the storage modulus and loss modulus gradually decrease in the yield stress area, it can be confirmed that there is no sudden change in material shape at the yield point. As the concentration of fumed silica increased, the yield stress of the matrix increased. In addition, both the storage and loss moduli of the matrix increased, but it could have resulted from the increased difference between the storage and loss moduli as the fumed silica increased. The closer the space between the particles of the fumed silica, the more the silicone oil is affected by the silicone surface, resulting in higher interactions.

The shear modulus and viscosity of a fumed silica/silicone oil matrix depended on the shear stress as well as the fumed silica content. In the process of passing the printer nozzle through the matrix, the crevasses created in the matrix collapses. However, after the printing material is injected, the matrix must maintain the shape of the printed features through its rapid recovery.[51] Figure 2f shows the creep and recovery characteristics of the matrix at higher shear forces due to low

https://doi.org/10.1021/acsomega.3c01165
ACS Omega 2023, 8, 23554−23565

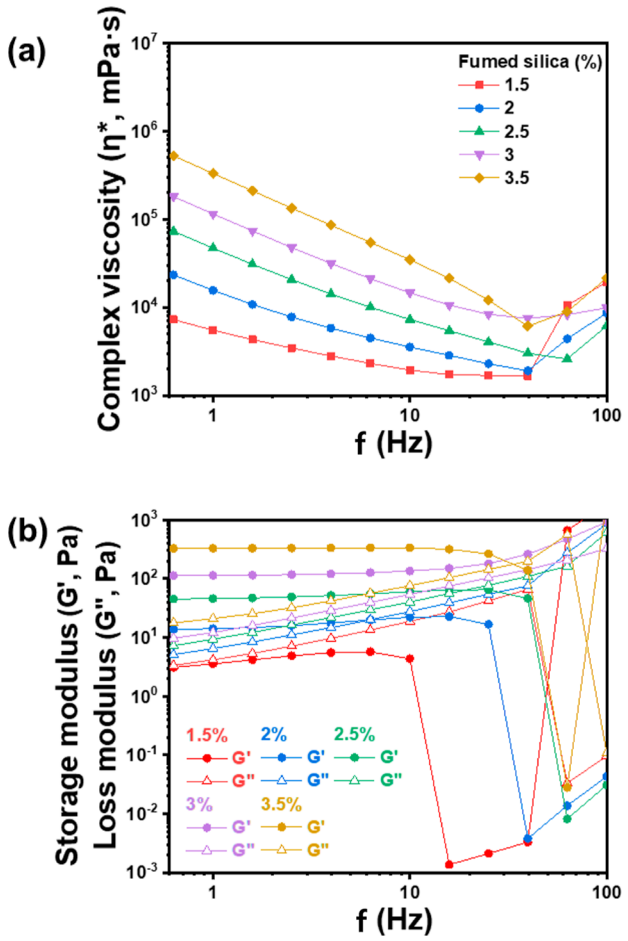

Figure 3. Rheological characterization of the fumed silica/silicone oil slurry supporter. (a) Viscosity of the supporter at different contents of fumed silica as a function of frequency. (b) Storage and loss moduli of supporters at different contents of fumed silica as a function of frequency.

moduli. The storage modulus of the samples was higher than the loss modulus at 0.5 Pa, while it was not completely recovered in the process of recovering from the 0.5 Pa state after the structure collapsed with a force of 300 Pa. The 2% fumed silica/silicone oil matrix had a loss modulus higher than the storage modulus. This result is the cause of the matrix not holding the material perfectly after printing. On the other hand, the matrix containing 2.5% fumed silica exhibited a slightly higher storage modulus than the loss modulus when exposed to a shear force of 0.5 Pa after receiving a shear of 300 Pa. In this state, the injected material can be preserved in a mild state. Fumed silica at 3 and 3.5% showed excellent recovery characteristics, but crevasses could be created in the matrix because the difference between the storage and the loss moduli was large. For 3 and 3.5% fumed silica formulations, its viscosity was too high that the crevasses remained for too long after the nozzle passed. In an ideal condition for DIW, the fumed silica slurries would return immediately to cover the pathway along with the nozzle. For the 3 and 3.5% formulations, the prints were highly affected and changed due to the formation of the crevasse, thus they were excluded from the study. Based on the rheological properties, it was considered that 2.5% of fumed silica was suitable for EMB3D printing with the fumed silica/silicone oil matrix.

3.2. Rheological Properties of the Photocurable Composite Resin. 2.5% fumed silica was used as the matrix for EMB3D, and a photocurable resin with SEP at different concentrations was used as a printing ink. Composite resins with nanomaterials show shear-thinning behavior.[52] The rheological behavior of the photocurable resin was investigated with the photocurable resin containing SEP at different concentrations (Figure 4). The composite photocurable resin showed Newtonian fluid behavior at concentrations of 0, 0.5, and 1 phr of SEP, while the shear-thinning behavior began at the concentration above 2 phr as illustrated in Figure 4a. The viscosity decreases and yield stress occurs as the structure of the nanostructure composed in a stationary state collapses, showing shear-thinning behavior (Figure 4b,c). Photocurable resins without SEP have a large amount of CTFA and IBOA, and only oligomer-like resins and some photoinitiators exist showing Newtonian fluid behavior. For low concentrations of 0.5 and 1 phr, both ends of the needle-shaped SEP do not interfere with each other, no matter which direction the SEP rotates in this state, no interference occurs. However, the movement of SEPs is interfered at higher concentrations and the percolation threshold appears. SEP 5 phr shows an entangled percolation critical point and produces an apparent shear-thinning behavior.

Figure 4d shows the yield characteristics of the photocurable SEP composite resin used in this experiment. The yield property of the matrix used in this experiment is important to maintain the shape of the printed material. However, the photocurable resin, which is the material to be printed, must always be present in a flowing state. Because, if this is not the case, even if problems do not occur in the EMB3D printing method, the output may not be performed in the DLP printing environment. However, as the content of SEP increases, the viscosity increases, so the yield characteristics must be checked. Significant graphs for yield characteristics were obtained from samples of 2, 3, and 5 phr of SEP content with shear-thinning characteristics. In the cases of 0, 0.5, and 1 phr, Newtonian fluid behavior was observed, so the yield characteristics were meaningless. From 2 to 5 phr, both the storage modulus and loss modulus increase with increasing SEP content. In addition, as the content increases, the difference between the storage modulus and the loss modulus narrows. However, it was confirmed that the loss modulus remained higher than the storage modulus in all samples and all sections of the shear force, and SEP remained flowing under 5 phr. Therefore, all samples are suitable for DLP and EMB3D printing.

As the shear modulus and viscosity of the fumed silica/silicone oil matrix in Figure 2e depend not only on the fumed silica content but also on the shear stress and time, Figures 4e and 5 also changes the shear modulus according to the SEP content, stress, and time. As can be seen in Figure 1−Figure 6, photocurable printing materials remain fluid before the UV radiation of DLP 3D printing. The storage modulus decreases at a shear force of 300 Pa but recovers at a shear force of 0.5 pa. However, during the test process, the material always maintains a loss modulus higher than the storage modulus.

Figure 6 is the result of monitoring the change in the storage modulus of photocurable composite resin during the curing process. After stabilizing the resin for 30 s, UV irradiation was performed. In general, the photocurable material to which the nanomaterial is added tends to be cured slowly because the nanomaterial absorbs UV.[17] The reason why photocuring occurs is important in the case of DLP-type 3D printing during

https://doi.org/10.1021/acsomega.3c01165
ACS Omega 2023, 8, 23554−23565

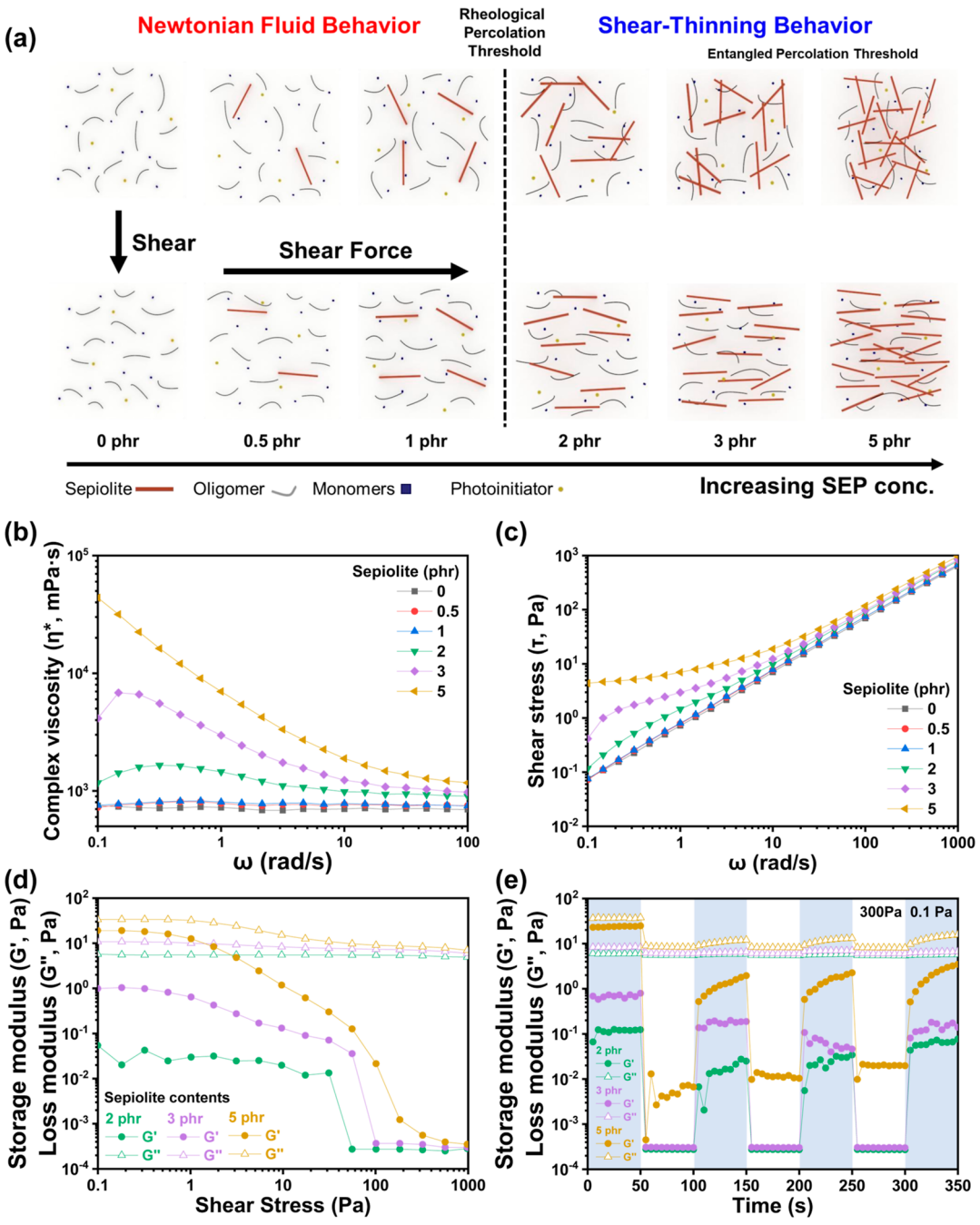

Figure 4. Rheological characterization of the photocurable resin composited with SEP. (a) Viscosity of the supporter at different contents of fumed silica as a function of the angular velocity. (b) Shear stress of the supporter at different contents of fumed silica as a function of the angular velocity. (c) Storage and loss moduli of supporters at different contents of fumed silica in stress sweeps. (d) Cyclic stress time sweep for 2, 2.5, 3, and 3.5 wt % supporting fumed silica/silicone oil gel. (e) For cyclic stress, the shaded regions were at a low stress of 0.1 Pa and the unshaded regions were at a high stress of 200 Pa.

the printing process. The time of UV irradiating the layer must be considered. If the curing behavior is delayed by SEP, different printing conditions should be applied for each sample. However, in Figure 6, it was confirmed that the storage modulus of all samples increased immediately after the UV irradiation. In addition, it was confirmed that as the content of SEP increased, the tendency of increasing the storage modulus of the material increased. From this phenomenon, it is considered that SEP has good compatibility with resin and is effective in supporting the structure.

3.3. Mechanical Properties of 3D-Printed Samples.

The main purpose of this experiment is to compare the physical properties of nanocomposites having orientation by 3D printing. As shown in Figure 7a,b, tensile strength samples were printed and tested using the DLP method (isotropic) and the EMB3D method (anisotropic). The experimental results of the DLP output sample show that the tensile strength and modulus of elasticity increase as the content of the SEP number increases. At a concentration of 5 phr, the tensile strength increases from 20.7 MPa (control, pure photocurable resin) to 25.6 MPa, and the modulus of elasticity increases

https://doi.org/10.1021/acsomega.3c01165
ACS Omega 2023, 8, 23554−23565

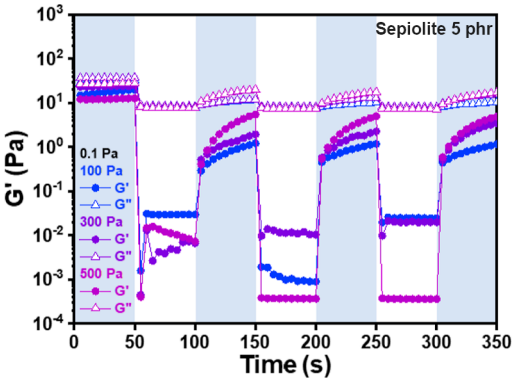

Figure 5. Storage and loss moduli of the supporter at different contents of SEP in a cyclic stress time sweep using 5 phr of resin. The unshaded regions were at a high stress of 100, 300, and 500 Pa.

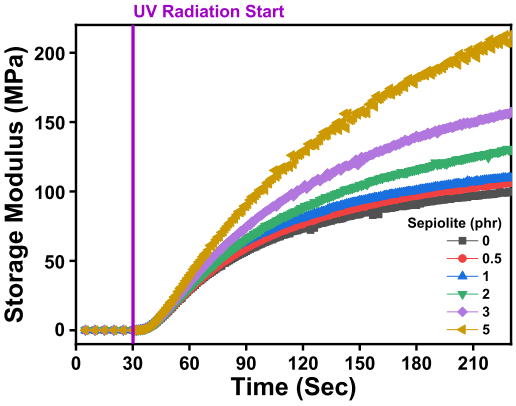

Figure 6. Change in the rheological properties of composites during UV irradiation by the SEP content.

from 210.9 MPa (control, pure photocurable resin) to 346.4 MPa. At the same time, it maintains the elongation at break of the sample despite increasing SEP loading, as shown in Figures 7e,f and 8. This phenomenon is presumed to be due to the characteristics of the acrylic resin used in this experiment. High-viscosity oligomers (GR30860, GR3060) used in the experiment and CTFA and IBOA used as monomers for viscosity dilution can respond to structural reinforcement and deformation through interaction with SEP with electrical attraction. If the mobility of the molecular chains of the polymer matrix of the nanocomposite is limited, the strength increases, but low elongation is produced. Similar experimental results have been reported previously.[9,38,53,54]

The tensile strength and modulus of elasticity of the sample printed by the EMB3D method are shown in Figure 7c,d. At a concentration of 5 phr, the tensile strength increases from 16.2 MPa (control, pure photocurable resin) to 27.2 MPa, and the modulus of elasticity increases from 123.6 MPa (control, pure photocurable resin) to 215.8 MPa. At the same time, as the SEP loading increases, the elongation at break of the sample also increases, as shown in Figures 7e,f and 8.

Pure photocurable resin printed with the DLP method shows higher tensile strength than pure photocurable resin printed with EMB3D. This can occur in the following phenomena. The process is inevitably separated by gaps,[55,56] creating voids that reduce the mechanical properties of the substrate. EMB3D-printed samples using pure photocurable resins are inferior to DLP-printed samples. However, one important point to note is that the strength does not increase consistently with increasing SEP content. From pure resin to 0.5 and 1 phr, the tensile strength increases with a slope similar to that of the DLP-type sample. However, the tensile strength increases very rapidly at 2 and 3 phr. This phenomenon can be interpreted in relation to the rheological behavior of photocurable resins containing SEP. This can happen in several phenomena. In Figure 4b,c, the rheological percolation threshold of photocurable resin can be identified. A material containing 0.5, 1 phr of pure resin and SEP shows Newtonian fluid behavior, and shear-thinning behavior appears above 2 phr. This behavior is consistent with the increase in tensile strength, and the SEP aligns with the shear-thinning behavior to reinforce the tensile strength. The EMB3D (anisotropic SEP) printing shows a higher increase than the increase in the tensile strength of DLP (isotropic SEP) printing. This study was conducted to enhance the mechanical properties of photocurable nanocomposites and to understand these synergies.

DMA was performed to measure the storage modulus of photo-cured acrylic resins and photo-cured nanocomposites. The storage modulus curves of the cured pure resin and SEP nanocomposites are shown in Figure 9a. The addition of a well-dispersed SEP greatly increases the storage modulus as the SEP content increases. The storage modulus of pure resin photocured at 25 °C is 194.9 MPa. As the SEP content increases, the storage modulus of composites tends to increase gradually. When the SEP content is 5 phr, the storage modulus is 267.3 MPa. The tan δ values representing the ratio of loss factor to storage factor for photo-cured pure resin and SEP nanocomposites are shown in Figure 9b. The maximum tan δ value of photo-cured pure resin is observed at 65.1 °C. It increases with increasing SEP content and is observed at 73.3 °C for 5 phr. In the glassy state, the storage coefficient of the SEP nanocomposite is higher than that of photo-cured pure resin, indicating that a well-dispersed mixed structure with good interfacial bonding improves the mechanical properties of the composite.

3.4. Morphological Properties of 3D-Printed Samples. The form of pure SEP before being dispersed in the photocurable resin is observed by SEM. As shown in Figure 10, the needle-shaped SEP particles are bundled and do not show the overall orientation. These SEM results are reported for comparison with photocurable resin/SEP composites. SEP's width and thickness are less than 20 nm, but its length is more than 100 nm, showing a very high aspect ratio. However, in the shape shown in Figure 10, the SEP is not separated into one unit. Bundles are observed to be agglomerated and look like pasta bundles. However, since SEP is easily separated by an external force such as tip sonication, it is easy to be used as a composite material in this experiment.

The tensile fracture surface of the photo-cured resin specimen printed by the DLP method is observed (Figure 11). In the high-magnification image, the polymer resin shows a very clean wave cross-section where no SEP is observed. The photocurable resin used in the research is a polymer with a complex network structure. When the shape changes mechanically by an external force, the structural arrangement of the polymer also changes (Figure 11a,b). This is because the photocurable resin of the same shape is present inside the material and flows in the deformation experiment at room temperature. As the temperature decreases or the tensile speed increases, the tensile fracture surface also changes shape. Figure

https://doi.org/10.1021/acsomega.3c01165
ACS Omega 2023, 8, 23554−23565

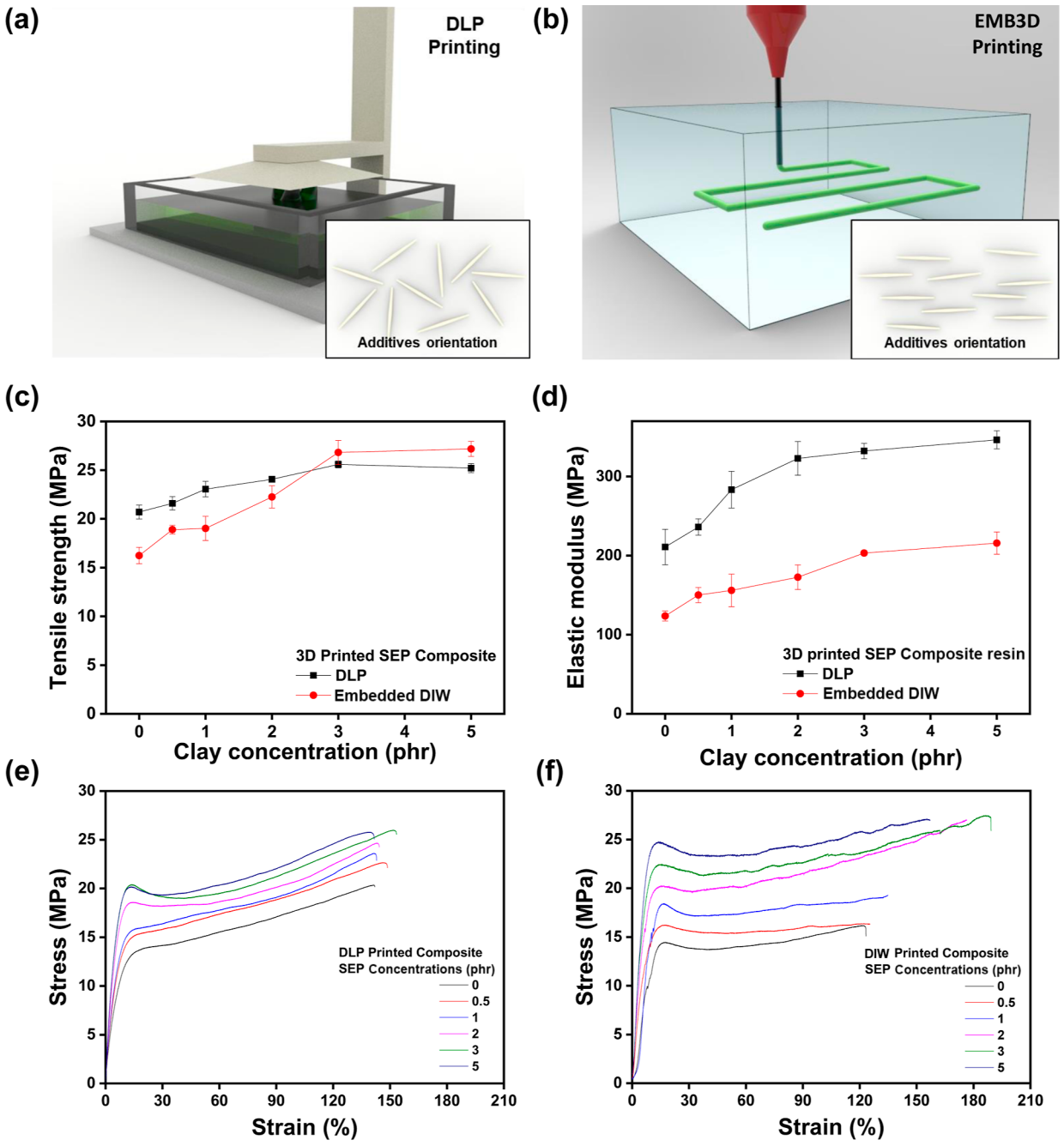

Figure 7. Change of tensile strength characteristics according to 3D printing methods. (a) DLP 3D printing and (b) EMB3D printing. Mechanical property measurements: (c) tensile strength and (d) Young's modulus of the photocurable composite resin with varying SEP concentrations. Stress strain graph of the sample output by (e) DLP and (f) EMB3D printing methods.

11c–f shows the tensile fracture surface of DLP-printed samples with SEP contents of 3 and 5 phr, respectively. The photo shows the irregular texture of the polymer, and the head and body of a SEP bundle are also observed. The irregular orientation of the SEP bundle can be deduced from the irregular distribution of the head and body shown in the photos in Figure 11d,f.

The tensile fracture surface of the photo-cured resin specimen printed by the EMB3D method is observed. The fractured part of the tensile sample printed in the vertical direction of the pure sighted resin is shown in Figure 12. Unlike the uneven surfaces of DLP samples, EMB3D-printed photocurable resins show very clean fracture surfaces. It is thought that the oligomers are arranged in the same direction as the photo-curable resin passes through the nozzle, forming a clean fracture surface. In addition, the SEP dispersed inside the resin also appears to have the same orientation as the printing direction. As the strongest evidence, both the head and body of SEP are observed in the tensile fracture surface of the sample printed by the DLP method, whereas in the case of the EMB3D-printed sample, only the head of the light is observed and not the lying body part (Figure 12).

The orientation of the SEP within the sample was observed based solely on the SEP particles exposed to the fracture surface. TEM images showed the distribution of SEP in the photo-cured resin produced using EMB3D printing (Figure

https://doi.org/10.1021/acsomega.3c01165
ACS Omega 2023, 8, 23554−23565

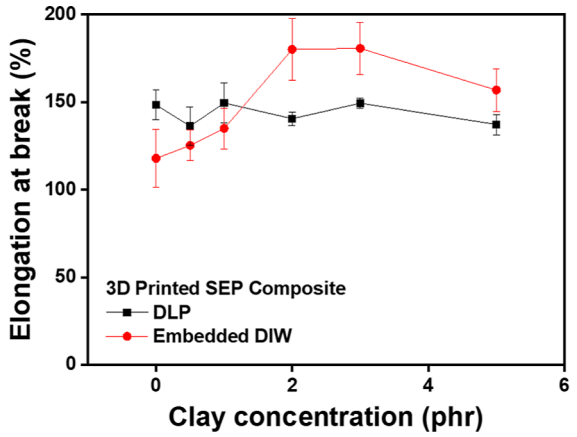

Figure 8. Mechanical property measurements of the elongation at break of nanocomposites with SEP at varying filler contents.

13). It can be confirmed that the SEP is well dispersed in the resin at a concentration of 5 phr. Interestingly, more than 30 particles all showed the same orientation in the sample, and the degree of orientation looked like an oriented strand board. As described above, the fluidity of the photocurable resin weakened the orientation of the SEP.

4. CONCLUSIONS

In this study, we demonstrated an experiment to create nano orientation properties of photocurable nanocomposites with low viscosity using EMB3D printing. In the conventional method of outputting DIW using a photocurable material and a nanomaterial composite material, there was a limitation in that low-concentration nanomaterials cannot be used. However, in this study, the rheological properties of using a fumed silica/silicone oil slurry as a matrix were studied in detail and optimal conditions were suggested. Using a fumed silica/silicone oil matrix, photocuring resin containing less than 5phr of SEP was printed by the EMB3D method. The samples printed by the EMB3D method were compared with those printed by the DLP method in terms of mechanical properties. As the amount of SEP increased, the mechanical tensile strength increased in both methods. However, it showed a higher reinforcing effect in reinforcing the mechanical properties of the material printed by the EMB3D method. In

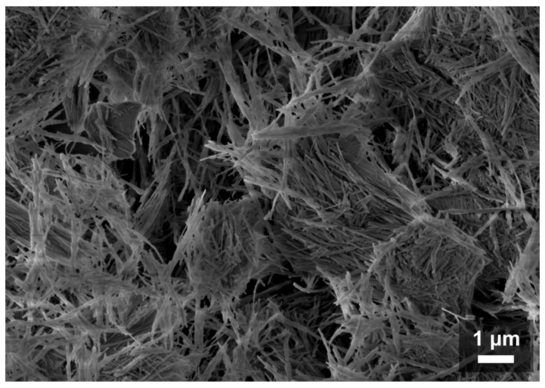

Figure 10. SEM image of the pure SEP powder.

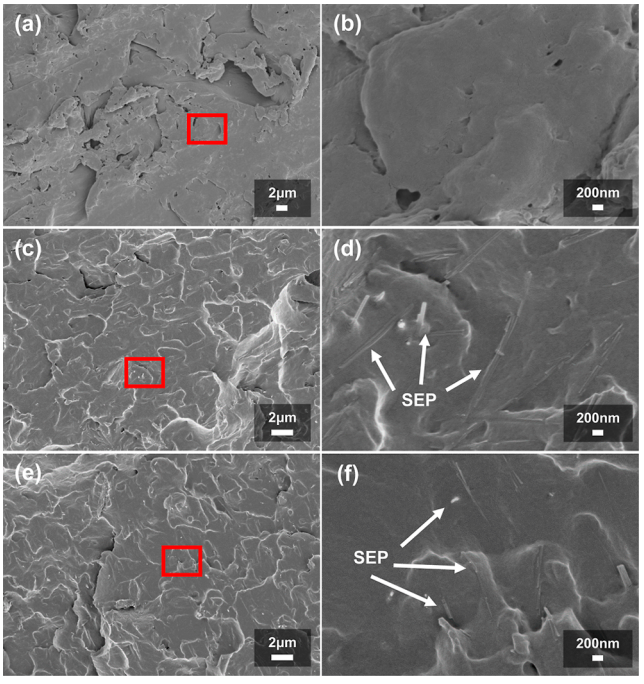

Figure 11. SEM image of post-tensile fracture surface observation of DLP 3D-printed polymer composites with tension applied. (a,b) Pure polymer, (c,d) SEP-3 composite, and (e,f) SEP-5 composite.

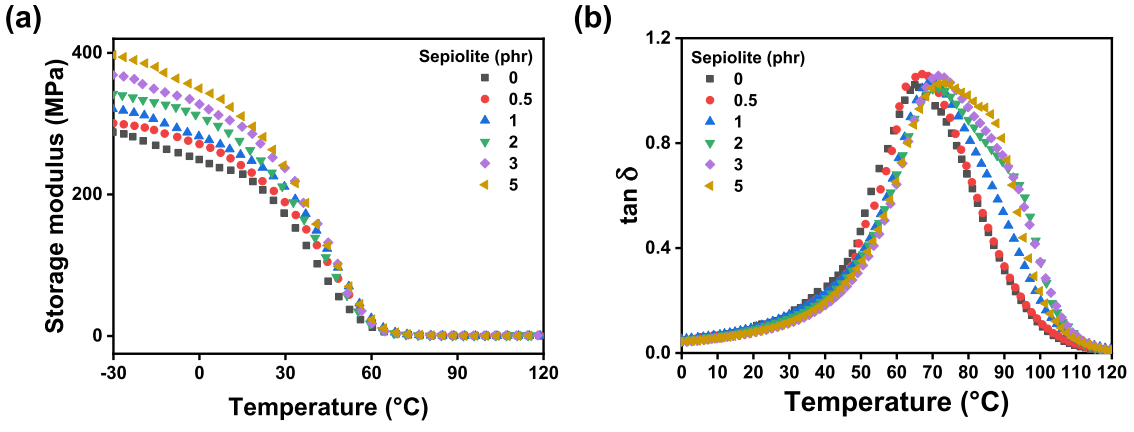

Figure 9. Process of manufacturing cured resin and resin-SEP nanocomposite and the rheological characterization of the materials. Temperature dependencies of (a) storage modulus G' and (b) tan δ (ratio of loss modulus to storage modulus) of pure cured resin and resin-SEP nanocomposites.

https://doi.org/10.1021/acsomega.3c01165
ACS Omega 2023, 8, 23554−23565

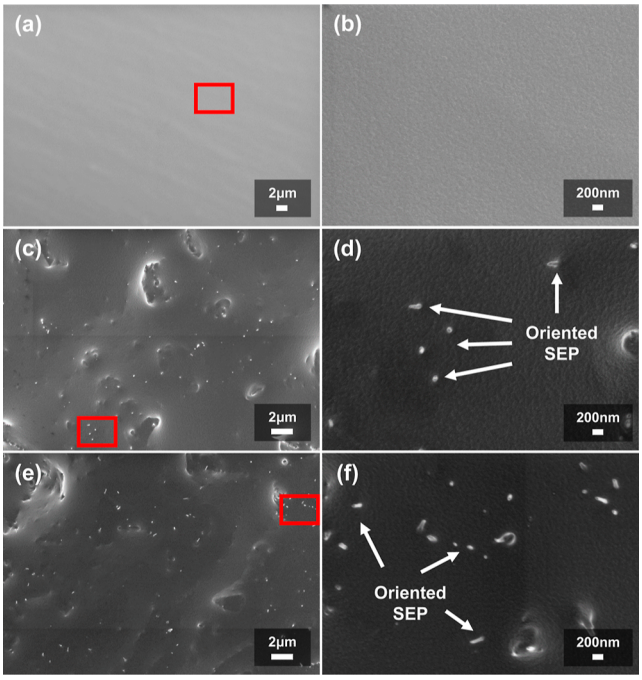

Figure 12. SEM image of post-tensile fracture surface observation of DIW 3D-printed polymer composites with tension applied. (a,b) Pure polymer, (c,d) SEP-3 composite, and (e, f) SEP-5 composite.

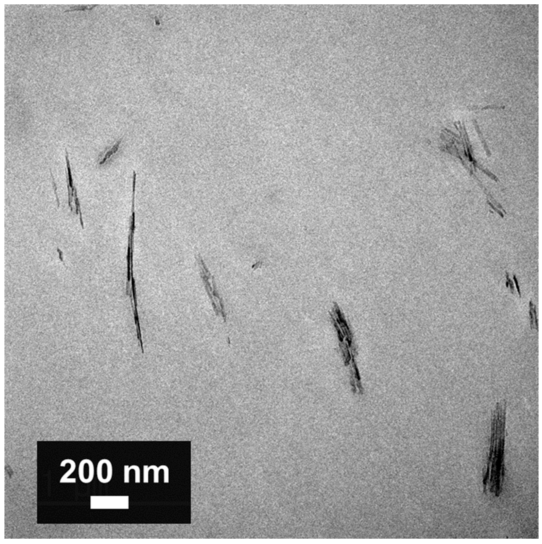

Figure 13. TEM image of oriented SEP particles in the DIW 3D-printed SEP-5 composite.

the process of passing the SEP through the printing nozzle, the material becomes oriented by receiving a shearing force, thereby enhancing the mechanical properties of the material more effectively. These physical properties were further strengthened at a concentration of 2 to 5 phr, which is the point at which the SEP contained in the photocurable resin begins to show shear-thinning. It was confirmed that this phenomenon is related to the rheological properties of the photocurable material containing SEP. In addition, the tensile fracture surfaces of the materials printed by DLP and EMB3D were compared. In the tensile fracture surface of the sample printed by DLP, the body part and the head part of the SEP were observed together, and in the case of the sample printed by EMB3D, only the head part of the SEP was observed. In addition, the degree of orientation of SEP was confirmed through TEM, and although the degree of orientation was not strong, it was confirmed that it exhibited a physical reinforcing effect. In addition, it was confirmed through DMA that there is compatibility between SEP and the acrylic monomer used. The low-concentration needle-shaped nanomaterials were first applied to EMB3D printing modified with the DIW method, and the rheological properties of the matrix and photocurable resin were also confirmed. This research is expected to serve as the basis for applying various nanomaterials, such as nanoclay, carbon nanotubes, and cellulose nanocrystals to EMB3D printing in the future. In particular, the low concentration of nanomaterials will make it possible to overcome the limitations of existing 3D printing materials with excellent physical reinforcement effects.

■ ASSOCIATED CONTENT

Supporting Information

The Supporting Information is available free of charge at https://pubs.acs.org/doi/10.1021/acsomega.3c01165.

Chemical structure of the acrylic monomers and photoinitiators; schematic of the chemical structure of SEP; 3D printing process and results; and TEM images of the oriented SEP particles (PDF)

■ AUTHOR INFORMATION

Corresponding Author

Hyun-Joong Kim − *Lab. of Adhesion & Bio-Composites, Program in Environmental Materials Science and Research Institute of Agriculture and Life Sciences, and Bioresources, Seoul National University, Seoul 08826, Republic of Korea;* orcid.org/0000-0002-3897-7939; Email: hjokim@snu.ac.kr; Fax: +82 28732318

Authors

Hoon Kim − *Lab. of Adhesion & Bio-Composites, Program in Environmental Materials Science, Seoul National University, Seoul 08826, Republic of Korea; Graphy Inc., Seoul 08826, Republic of Korea;* orcid.org/0000-0002-4447-4553

Jaehwan Kim − *Program in Biosystems and Biomaterials Science and Engineering, Seoul National University, Seoul 08826, Republic of Korea*

Kwang-Hyun Ryu − *Lab. of Adhesion & Bio-Composites, Program in Environmental Materials Science, Seoul National University, Seoul 08826, Republic of Korea*

Jiho Lee − *Graphy Inc., Seoul 08826, Republic of Korea;* orcid.org/0000-0003-2408-2808

Jinho Hyun − *Program in Biosystems and Biomaterials Science and Engineering and Research Institute of Agriculture and Life Sciences, and Bioresources, Seoul National University, Seoul 08826, Republic of Korea;* orcid.org/0000-0002-9992-5681

Jaseung Koo − *Department of Organic Materials Engineering, Chungnam National University, Daejeon 34134, Republic of Korea;* orcid.org/0000-0002-3646-0805

Complete contact information is available at: https://pubs.acs.org/10.1021/acsomega.3c01165

Notes

The authors declare no competing financial interest.

https://doi.org/10.1021/acsomega.3c01165
ACS Omega 2023, 8, 23554−23565

■ ACKNOWLEDGMENTS

This work was supported by the Technology Development Program(S3145666) funded by the Ministry of SMEs and Startups (MSS, Korea).

■ REFERENCES

(1) Jones, N. Science in Three Dimensions: The Print Revolution. *Nature* **2012**, *487*, 22−23.
(2) Truby, R. L.; Lewis, J. A. Printing Soft Matter in Three Dimensions. *Nature*; Nature Publishing Group December, 2016; Vol. *14*, pp 371−378.
(3) Kim, H.; Ryu, K.-H.; Baek, D.; Khan, T. A.; Kim, H.-J.; Shin, S.; Hyun, J.; Ahn, J. S.; Ahn, S.-J.; Kim, H. J.; Koo, J. 3D Printing of Polyethylene Terephthalate Glycol−Sepiolite Composites with Nanoscale Orientation. *ACS Appl. Mater. Interfaces* **2020**, *12*, 23453−23463.
(4) Tian, X.; Liu, T.; Yang, C.; Wang, Q.; Li, D. Interface and Performance of 3D Printed Continuous Carbon Fiber Reinforced PLA Composites. *Compos. Part A Appl. Sci. Manuf.* **2016**, *88*, 198−205.
(5) Ngo, T. D.; Kashani, A.; Imbalzano, G.; Nguyen, K. T. Q.; Hui, D. Additive Manufacturing (3D Printing): A Review of Materials, Methods, Applications and Challenges. *Composites Part B: Engineering*; Elsevier Ltd June, 2018; Vol. *15*, pp 172−196.
(6) Markstedt, K.; Escalante, A.; Toriz, G.; Gatenholm, P. Biomimetic Inks Based on Cellulose Nanofibrils and Cross-Linkable Xylans for 3D Printing. *ACS Appl. Mater. Interfaces* **2017**, *9*, 40878−40886.
(7) Dubey, N.; Ferreira, J. A.; Malda, J.; Bhaduri, S. B.; Bottino, M. C. Extracellular Matrix/Amorphous Magnesium Phosphate Bioink for 3D Bioprinting of Craniomaxillofacial Bone Tissue. *ACS Appl. Mater. Interfaces* **2020**, *12*, 23752−23763.
(8) Nadgorny, M.; Ameli, A. Functional Polymers and Nanocomposites for 3D Printing of Smart Structures and Devices. *ACS Applied Materials and Interfaces*. *American Chemical Society May* **2018**, *10*, 17489−17507.
(9) Chen, Q.; Mangadlao, J. D.; Wallat, J.; De Leon, A.; Pokorski, J. K.; Advincula, R. C. 3D Printing Biocompatible Polyurethane/Poly(Lactic Acid)/Graphene Oxide Nanocomposites: Anisotropic Properties. *ACS Appl. Mater. Interfaces* **2017**, *9*, 4015−4023.
(10) Bhandari, S.; Lopez-Anido, R. A.; Gardner, D. J. Enhancing the Interlayer Tensile Strength of 3D Printed Short Carbon Fiber Reinforced PETG and PLA Composites via Annealing. *Addit. Manuf.* **2019**, *30*, 100922.
(11) Gul, J. Z.; Sajid, M.; Choi, K. H. 3D Printed Highly Flexible Strain Sensor Based on TPU-Graphene Composite for Feedback from High Speed Robotic Applications. *J. Mater. Chem. C* **2019**, *7*, 4692−4701.
(12) Singh, S.; Ramakrishna, S.; Berto, F. 3D Printing of Polymer Composites: A Short Review. *Mater. Des. Process. Commun.* **2020**, *2*(), DOI: 10.1002/mdp2.97.
(13) Park, Y. G.; Min, H.; Kim, H.; Zhexembekova, A.; Lee, C. Y.; Park, J. U. Three-Dimensional, High-Resolution Printing of Carbon Nanotube/Liquid Metal Composites with Mechanical and Electrical Reinforcement. *Nano Lett.* **2019**, *19*, 4866−4872.
(14) Guvendiren, M.; Molde, J.; Soares, R. M. D.; Kohn, J. Designing Biomaterials for 3D Printing *ACS Biomaterials Science and Engineering*; American Chemical Society October, 2016; Vol. *10*, pp 1679−1693
(15) Palaganas, N. B.; Mangadlao, J. D.; De Leon, A. C. C.; Palaganas, J. O.; Pangilinan, K. D.; Lee, Y. J.; Advincula, R. C. 3D Printing of Photocurable Cellulose Nanocrystal Composite for Fabrication of Complex Architectures via Stereolithography. *ACS Appl. Mater. Interfaces* **2017**, *9*, 34314−34324.
(16) Palaganas, J. O.; Palaganas, N. B.; Ramos, L. J. I.; David, C. P. C. 3D Printing of Covalent Functionalized Graphene Oxide Nanocomposite via Stereolithography. *ACS Appl. Mater. Interfaces* **2019**, *11*, 46034−46043.
(17) Weng, Z.; Zhou, Y.; Lin, W.; Senthil, T.; Wu, L. Structure-Property Relationship of Nano Enhanced Stereolithography Resin for Desktop SLA 3D Printer. *Compos. Part A Appl. Sci. Manuf.* **2016**, *88*, 234−242.
(18) Kim, H.; Park, J.-W.; Kim, H.-J. Flame Retardant Nanocomposites Containing Nano-Fillers. In *Science and applications of Tailored Nanostructures*; Paolo, D. S., Ed.; onecentralpress, 2017, pp 1−28.
(19) Del Río, M. S.; García-Romero, E.; Suárez, M.; Da Silva, I.; Fuentes-Montero, L.; Martínez-Criado, G. Variability in Sepiolite: Diffraction Studies. *Am. Mineral.* **2011**, *96*, 1443−1454.
(20) Tabatabaei-Yazdi, Z.; Mehdipour-Ataei, S. Poly(Ether-Imide) and Related Sepiolite Nanocomposites: Investigation of Physical, Thermal, and Mechanical Properties. *Polym. Adv. Technol.* **2015**, *26*, 308−314.
(21) Gratson, G. M.; Lewis, J. A. Phase Behavior and Rheological Properties of Polyelectrolyte Inks for Direct-Write Assembly. *Langmuir* **2005**, *21*, 457−464.
(22) Markstedt, K.; Mantas, A.; Tournier, I.; Martínez Ávila, H.; Hägg, D.; Gatenholm, P. 3D Bioprinting Human Chondrocytes with Nanocellulose-Alginate Bioink for Cartilage Tissue Engineering Applications. *Biomacromolecules* **2015**, *16*, 1489−1496.
(23) Lewis, J. A.; Gratson, G. M. Direct Writing in Three Dimensions. *Mater Today* **2004**, *7*, 32−39.
(24) Zhou, L.; Fu, J.; He, Y. A Review of 3D Printing Technologies for Soft Polymer Materials. *Adv. Funct. Mater.* **2020**, *30*, 2000187.
(25) Zhang, Y.; Yin, X. Y.; Zheng, M.; Moorlag, C.; Yang, J.; Wang, Z. L. 3D Printing of Thermoreversible Polyurethanes with Targeted Shape Memory and Precise in Situ Self-Healing Properties. *J. Mater. Chem. A* **2019**, *7*, 6972−6984.
(26) Kuang, X.; Chen, K.; Dunn, C. K.; Wu, J.; Li, V. C. F.; Qi, H. J. 3D Printing of Highly Stretchable, Shape-Memory, and Self-Healing Elastomer toward Novel 4D Printing. *ACS Appl. Mater. Interfaces* **2018**, *10*, 7381−7388.
(27) Barry, R. A.; Shepherd, R. F.; Hanson, J. N.; Nuzzo, R. G.; Wiltzius, P.; Lewis, J. A. Direct-Write Assembly of 3D Hydrogel Scaffolds for Guided Cell Growth. *Adv. Mater.* **2009**, *21*, 2407−2410.
(28) Valentine, A. D.; Busbee, T. A.; Boley, J. W.; Raney, J. R.; Chortos, A.; Kotikian, A.; Berrigan, J. D.; Durstock, M. F.; Lewis, J. A. Hybrid 3D Printing of Soft Electronics. *Adv. Mater.* **2017**, *29*, 1703817.
(29) Derakhshanfar, S.; Mbeleck, R.; Xu, K.; Zhang, X.; Zhong, W.; Xing, M.. 3D Bioprinting for Biomedical Devices and Tissue Engineering: A Review of Recent Trends and Advances. *Bioactive Materials*; KeAi Communications Co. June, 2018; Vol. *1*, pp 144−156
(30) Yuk, H.; Lu, B.; Lin, S.; Qu, K.; Xu, J.; Luo, J.; Zhao, X. 3D Printing of Conducting Polymers. *Nat. Commun.* **2020**, *11*, 1604.
(31) Orangi, J.; Hamade, F.; Davis, V. A.; Beidaghi, M. 3D Printing of Additive-Free 2D Ti3C2Tx (MXene) Ink for Fabrication of Micro-Supercapacitors with Ultra-High Energy Densities. *ACS Nano* **2020**, *14*, 640−650.
(32) Kokkinis, D.; Schaffner, M.; Studart, A. R. Multimaterial Magnetically Assisted 3D Printing of Composite Materials. *Nat. Commun.* **2015**, *6*, 8643.
(33) Li, V. C. F.; Dunn, C. K.; Zhang, Z.; Deng, Y.; Qi, H. J. Direct Ink Write (DIW) 3D Printed Cellulose Nanocrystal Aerogel Structures. *Sci. Rep.* **2017**, *7*, 8018.
(34) Cheng, Y.; Chan, K. H.; Wang, X. Q.; Ding, T.; Li, T.; Lu, X.; Ho, G. W. Direct-Ink-Write 3D Printing of Hydrogels into Biomimetic Soft Robots. *ACS Nano* **2019**, *13*, 13176−13184.
(35) Tang, X.; Zhou, H.; Cai, Z.; Cheng, D.; He, P.; Xie, P.; Zhang, D.; Fan, T. Generalized 3D Printing of Graphene-Based Mixed-Dimensional Hybrid Aerogels. *ACS Nano* **2018**, *12*, 3502−3511.
(36) Lewis, J. A. Direct Ink Writing of 3D Functional Materials. *Adv. Funct. Mater.* **2006**, *16*, 2193−2204.
(37) Leppiniemi, J.; Lahtinen, P.; Paajanen, A.; Mahlberg, R.; Metsä-Kortelainen, S.; Pinomaa, T.; Pajari, H.; Vikholm-Lundin, I.; Pursula, P.; Hytönen, V. P. 3D-Printable Bioactivated Nanocellulose-Alginate Hydrogels. *ACS Appl. Mater. Interfaces* **2017**, *9*, 21959−21970.

https://doi.org/10.1021/acsomega.3c01165
ACS Omega 2023, 8, 23554−23565

(38) Siqueira, G.; Kokkinis, D.; Libanori, R.; Hausmann, M. K.; Gladman, A. S.; Neels, A.; Tingaut, P.; Zimmermann, T.; Lewis, J. A.; Studart, A. R. Cellulose Nanocrystal Inks for 3D Printing of Textured Cellular Architectures. *Adv. Funct. Mater.* **2017**, *27*, 1604619.
(39) Hausmann, M. K.; Rühs, P. A.; Siqueira, G.; Läuger, J.; Libanori, R.; Zimmermann, T.; Studart, A. R. Dynamics of Cellulose Nanocrystal Alignment during 3D Printing. *ACS Nano* **2018**, *12*, 6926−6937.
(40) Cho, J.; Jeon, I.; Kim, S. Y.; Lim, S.; Jho, J. Y. Improving Dispersion and Barrier Properties of Polyketone/Graphene Nanoplatelet Composites via Noncovalent Functionalization Using Aminopyrene. *ACS Appl. Mater. Interfaces* **2017**, *9*, 27984−27994.
(41) Khoshkava, V.; Kamal, M. R. Effect of Cellulose Nanocrystals (CNC) Particle Morphology on Dispersion and Rheological and Mechanical Properties of Polypropylene/CNC Nanocomposites. *ACS Appl. Mater. Interfaces* **2014**, *6*, 8146−8157.
(42) Karyappa, R.; Ching, T.; Hashimoto, M. Embedded Ink Writing (EIW) of Polysiloxane Inks. *ACS Appl. Mater. Interfaces* **2020**, *12*, 23565−23575.
(43) Grosskopf, A. K.; Truby, R. L.; Kim, H.; Perazzo, A.; Lewis, J. A.; Stone, H. A. Viscoplastic Matrix Materials for Embedded 3D Printing. *ACS Appl. Mater. Interfaces* **2018**, *10*, 23353−23361.
(44) Hu, S.-W.; Sung, P.-J.; Nguyen, T. P.; Sheng, Y.-J.; Tsao, H.-K. UV-Resistant Self-Healing Emulsion Glass as a New Liquid-like Solid Material for 3D Printing. *ACS Appl. Mater. Interfaces* **2020**, *12*, 24450−24457.
(45) Shin, S.; Hyun, J. Matrix-Assisted Three-Dimensional Printing of Cellulose Nanofibers for Paper Microfluidics. *ACS Appl. Mater. Interfaces* **2017**, *9*, 26438−26446.
(46) Jin, Y.; Compaan, A.; Chai, W.; Huang, Y. Functional Nanoclay Suspension for Printing-Then-Solidification of Liquid Materials. *ACS Appl. Mater. Interfaces* **2017**, *9*, 20057−20066.
(47) Leblanc, K. J.; Niemi, S. R.; Bennett, A. I.; Harris, K. L.; Schulze, K. D.; Sawyer, W. G.; Taylor, C.; Angelini, T. E. Stability of High Speed 3D Printing in Liquid-Like Solids. *ACS Biomater. Sci. Eng.* **2016**, *2*, 1796−1799.
(48) Muth, J. T.; Vogt, D. M.; Truby, R. L.; Mengüç, Y.; Kolesky, D. B.; Wood, R. J.; Lewis, J. A. Embedded 3D Printing of Strain Sensors within Highly Stretchable Elastomers. *Adv. Mater.* **2014**, *26*, 6307−6312.
(49) Cain, J. D.; Azizi, A.; Maleski, K.; Anasori, B.; Glazer, E. C.; Kim, P. Y.; Gogotsi, Y.; Helms, B. A.; Russell, T. P.; Zettl, A. Sculpting Liquids with Two-Dimensional Materials: The Assembly of $Ti_3C_2T_{<i>x</i>}$ MXene Sheets at Liquid−Liquid Interfaces. *ACS Nano* **2019**, *13*, 12385−12392.
(50) Jim, C. Y. Impregnation of Moist and Dry Unconsolidated Clay Samples Using Spurr Resin for Microstructural Studies. *J. Sediment. Res.* **1985**, *55*, 597−599.
(51) Bhattacharjee, T.; Zehnder, S. M.; Rowe, K. G.; Jain, S.; Nixon, R. M.; Sawyer, W. G.; Angelini, T. E. Writing in the Granular Gel Medium. *Sci. Adv.* **2015**, *1*, No. e1500655.
(52) Kim, H.; Ryu, K. H.; Baek, D.; Khan, T. A.; Kim, H. J.; Shin, S.; Hyun, J.; Ahn, J. S.; Ahn, S. J.; Kim, H. J.; Koo, J. 3D Printing of Polyethylene Terephthalate Glycol-Sepiolite Composites with Nanoscale Orientation. *ACS Appl. Mater. Interfaces* **2020**, *12*, 23453−23463.
(53) Gnanasekaran, K.; Heijmans, T.; van Bennekom, S.; Woldhuis, H.; Wijnia, S.; de With, G.; Friedrich, H. 3D Printing of CNT- and Graphene-Based Conductive Polymer Nanocomposites by Fused Deposition Modeling. *Appl. Mater. Today* **2017**, *9*, 21−28.
(54) Liu, Y.; Kumar, S. Polymer/Carbon Nanotube Nano Composite Fibers-A Review. *ACS Applied Materials and Interfaces*; American Chemical Society, 2014; Vol. *6*, pp 6069−6087.
(55) Tekinalp, H. L.; Kunc, V.; Velez-Garcia, G. M.; Duty, C. E.; Love, L. J.; Naskar, A. K.; Blue, C. A.; Ozcan, S. Highly Oriented Carbon Fiber-Polymer Composites via Additive Manufacturing. *Compos. Sci. Technol.* **2014**, *105*, 144−150.
(56) Blok, L. G.; Longana, M. L.; Yu, H.; Woods, B. K. S. An Investigation into 3D Printing of Fibre Reinforced Thermoplastic Composites. *Addit. Manuf.* **2018**, *22*, 176−186.

https://doi.org/10.1021/acsomega.3c01165
ACS Omega 2023, 8, 23554−23565